THE JOURNAL OF PHYSICAL CHEMISTRY A

Article

pubs.acs.org/JPCA

Influence of Intense THz Radiation on Spin State of Photoswitchable Compound $Cu(hfac)_2L^{Pr}$

Sergey L. Veber,*[,†] Matvey V. Fedin,[†] Ksenia Yu. Maryunina,[†] Kirill N. Boldyrev,[‡] Mikhail A. Sheglov,[§] Vitaly V. Kubarev,[§,∥] Oleg A. Shevchenko,[§] Nikolay A. Vinokurov,[§] Gennady N. Kulipanov,[§] Renad Z. Sagdeev,[†] Victor I. Ovcharenko,[†] and Elena G. Bagryanskaya[†,⊥]

[†]International Tomography Center, SB RAS, 630090 Novosibirsk, Russia

[‡]Institute of Spectroscopy RAS, 142190 Troitsk, Russia

[§]Budker Institute of Nuclear Physics, SB RAS, 630090 Novosibirsk, Russia

[∥]Novosibirsk State University, Novosibirsk 630090, Russia

[⊥]N.N. Vorozhtsov Novosibirsk Institute of Organic Chemistry, SB RAS, 630090 Novosibirsk, Russia

Supporting Information

ABSTRACT: The family of magnetoactive compounds $Cu(hfac)_2L^R$ exhibits thermo- and photoswitching phenomena promising for various applications. Photoswitching of the $Cu(hfac)_2L^{Pr}$ compound can be observed at temperatures below 20 K and is accompanied by transition to metastable structural state. Reverse conversion to stable structure could not be induced by light of near-IR−vis−UV regions up to date. The far-IR spectra of metastable and stable structural states are different and show characteristic absorption lines in the range of 170−240 cm^{-1}. These frequencies are accessible by NovoFEL − high-power THz free-electron laser user facility in Novosibirsk. We investigate selective influence of THz radiation on relaxation processes from metastable to stable structural state, which can be monitored by electron paramagnetic resonance (EPR). For this purpose, the experimental station based on X-band EPR spectrometer has been constructed by the THz beamline of NovoFEL and equipped with multimodal THz waveguide allowing to fed radiation directly into the EPR resonator. It has been found that irradiation of studied compound with high-power THz light causes significant but nondestructive increase of its temperature. Apart from this effect, no resonant influence of THz irradiation on relaxation processes has been observed. The experimental results have been rationalized taking into account vibrational relaxation times of the studied compound. Further experiments based on pulse heating by THz radiation have been proposed.

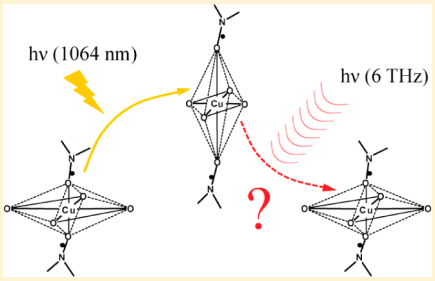

INTRODUCTION

Design of magnetic compounds with unusual properties has been the topic of many joint efforts of chemists and physicists during recent decades.[1−6] The compounds exhibiting thermo- or photoswitching phenomena have been studied most actively due to their potential applications in spintronics.[7−10] Magnetic compounds based on transition metals bridged by nitroxide radicals as spin carriers are promising systems, which require further investigation due to the variety of their magnetic properties.[11,12] Versatile magnetic behaviors found in copper(II)-nitroxide complexes strongly depend on coordination geometry of copper(II) ion. In the case of axially coordinated nitroxide radical, the exchange interaction copper(II)-nitroxide is weak and ferromagnetic.[13−15] In contrast, an equatorial coordination results in a strong antiferomagnetic coupling between copper(II) and nitroxide.[16,17] A new type of copper(II)-nitroxide complexes undergoing conversion between these two possible coordination geometries with temperature has been discovered and characterized.[18] Because of the axial-to-equatorial conversion, the copper(II)−nitroxide interaction in these compounds is significantly different at temperatures above and below phase transition, as has been shown in magnetic susceptibility studies. At the same time, significant structural rearrangements during phase transition require high mechanical stability of the crystals, for example, single crystals of compound discussed in ref 18, usually broke on cooling to the phase-transition temperature, which made their structural study using X-ray analysis complicated or impossible.[18,19]

Molecular magnets $Cu(hfac)_2L^R$ ("breathing crystals") based on copper(II) hexafluoroacetylacetonates ($Cu(hfac)_2$) and pyrazolyl-substituted nitronylnitroxides (L^R) have polymer-chain structure and demonstrate similar magnetic effects but occurring without crystal destruction.[20−23] The compound $Cu(hfac)_2L^{Pr}$ (Pr = propyl) studied in this work has a "head-to-head" coordination motif with CuO_6 units (spin triads) and CuO_4N_2 (one-spin) units alternating along the polymer chain (Figure 1a). The X-ray study and magnetic susceptibility

Received: November 19, 2012
Revised: January 16, 2013
Published: January 18, 2013

   dx.doi.org/10.1021/jp311404t | J. Phys. Chem. A 2013, 117, 1483−1491

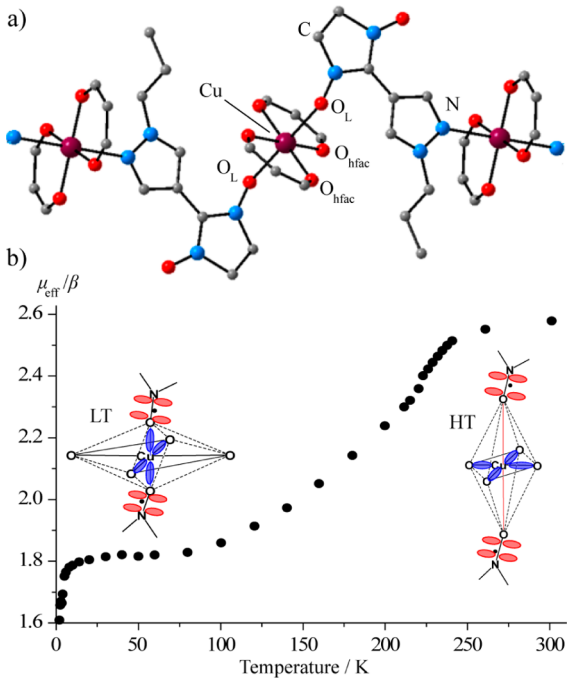

Figure 1. (a) Polymer-chain structure of the $Cu(hfac)_2L^{Pr}$ complex and (b) temperature dependence of its effective magnetic moment. Insets show the geometry of three-spin cluster above and below phase transition. Localization of unpaired electrons is depicted.

measurements of these compounds showed that the main rearrangements responsible for significant changes of the effective magnetic moment are localized in the CuO_6 units containing the nitroxide-copper(II)-nitroxide spin triads (Figure 1b).[21] At high temperatures ($T \approx 293$ K) coordination octahedra CuO_6 are elongated along the direction of O_L–Cu–O_L axis containing oxygens of nitroxide radicals.

As the temperature is lowered from 293 to 90 K, X-ray data indicate shortening of the O_L–Cu-O_L axis and simultaneous lengthening of one of the O_{hfac}–Cu–O_{hfac} axes. As a result, the nitroxides pass from axial (high-temperature (HT) geometry) to equatorial (low-temperature (LT) geometry) coordination positions of copper(II) ion (Figure 1b, insets). This rearrangement is accompanied by a switch of exchange interaction in spin triad nitroxide-copper(II)-nitroxide from weak ferromagnetic to a strong antiferromagnetic due to redistribution of the spin density of unpaired electron in copper(II) unit. In agreement with this structural data, the value of the effective magnetic moment of $Cu(hfac)_2L^{Pr}$ at room temperature corresponds to three weakly coupled spins of a triad. As the temperature is decreased, the magnetic moment drops down corresponding to effective coupling of two spins of three in exchange-coupled spin triads. As follows from $\mu_{eff}(T)$ dependence, the spin state conversion of $Cu(hfac)_2L^{Pr}$ is essentially completed at $T < 100$ K. Further decrease in the effective magnetic moment at cryogenic temperature is caused by intercluster exchange interaction between spin triads of different polymer chains.[24]

Along with X-ray and magnetic susceptibility measurements, the EPR is a choice technique for studying breathing crystals.[25−32] At temperatures above spin transition (HT geometry), the EPR signal of spin triad in the polycrystalline powder spectrum of $Cu(hfac)_2L^{R}$ is superimposed with the signal of magnetically isolated one-spin copper(II) units and consists of a single broad isotropic line with $g > 2$ (Figure 2a). The intracluster exchange interaction is weak at HT geometry;

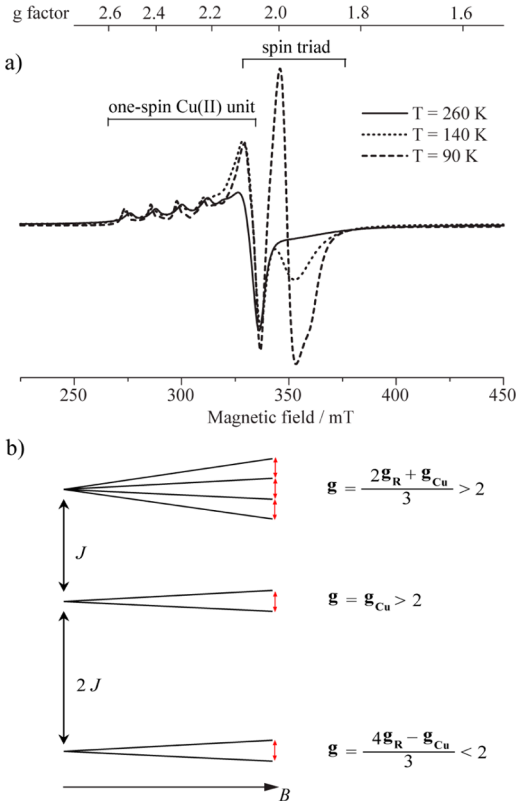

Figure 2. (a) EPR spectra of polycrystalline powder sample of $Cu(hfac)_2L^{Pr}$ at different temperature (adapted from ref 25) and (b) scheme of energy levels of spin triad and corresponding g-tensors of spin multiplets. Red arrows indicate allowed EPR transitions.

therefore, all multiplets of spin triad are populated (Figure 2b) and the EPR signal is characterized by averaged g-tensors of copper(II) and two nitroxides.

At temperatures below spin transition (LT geometry), only the lowest spin multiplet is populated due to the strong antiferromagnetic exchange interaction (Figure 2b), and the spectrum of spin triad shows powder pattern with all components of g-tensor being less than 2. Thus, HT (weakly coupled spin state) and LT (strongly coupled spin state) geometries of spin triad can be reliably distinguished using EPR.

It has also been shown that breathing crystals are capable of light-induced switching at cryogenic temperatures (below 20 K).[33] Under irradiation with light, the three-spin triad switches from stable strongly coupled spin state (LT geometry) to metastable weakly coupled spin state (HT geometry), which will be referred to as the ground (**G**) and metastable (**M**) states below, respectively. The rate of the reverse **M**→**G** relaxation strongly depends on temperature: at 4 to 5 K complete relaxation takes several hours, whereas at $T > 20$ K it occurs on the subsecond time scale and cannot be detected using continuous-wave (CW) EPR. A detailed investigation of relaxation **M**→**G** for several compounds of breathing crystals family revealed its unusual self-decelerating character, which can be explained by a broad distribution of relaxation parameters in **M** state.[34] Recent W-band time-resolved EPR study revealed that the formation of **M** state takes less than 100

dx.doi.org/10.1021/jp311404t | J. Phys. Chem. A 2013, 117, 1483−1491

ns (faster than the resolution time of the technique used).[35] It has also been found that the excitation of MLCT or d-d transitions of either **G** or **M** states leads to preferential formation of the **M** state; this probably is the main reason why it was so far impossible to perform reverse light-induced switching **M**→**G**. Up to date, temperature -induced relaxation has been the only known way to convert the metastable **M** state of the triad back to the ground **G** state.

At the same time, the low-energy barrier between **M** and **G** states (E_A = 19 ± 5K, Figure 3a)[34] seems promising for

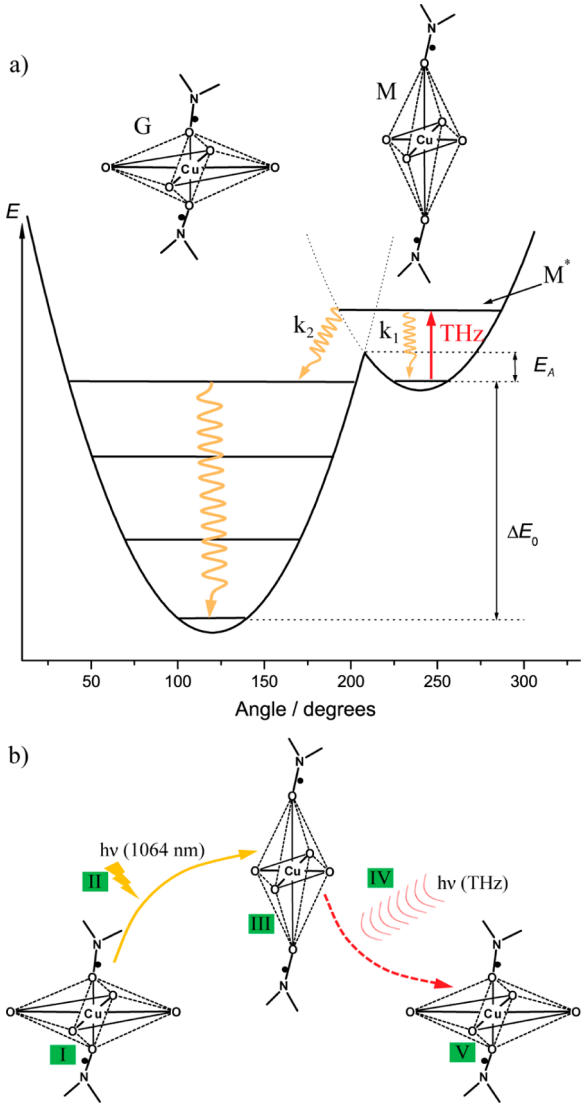

Figure 3. (a) Schematic circular section of the potential energy surface associated with the two Jahn–Teller valleys in breathing crystals. Structures corresponding to ground (**G**) and metastable (**M**) geometries are sketched on top. Expected mechanism of reverse conversion by THz radiation is shown. (b) Experimental procedure used in investigation of the influence of THz radiation on spin triads in photoinduced **M** state.

inducing reverse switching of the cluster by "soft" THz irradiation (Figure 3a, red arrow) and avoiding the excitation to higher energy MLCT or d-states. Indeed, the excitation of the cluster to one of the nonzero vibrational levels (**M**→**M***) by THz radiation will subsequently induce **M***→**G** conversion (Figure 3a). The efficiency of conversion depends on the ratio k_2/k_1, where k_1 characterizes the rate of vibrational relaxation **M***→**M**, and k_2 describes the **M***→**G** conversion. Thus, if $k_1 < k_2$, then one would expect the acceleration of **M**→**G** relaxation when the resonant (to **M**→**M*** transition) THz power is applied.

Synchrotrons and free electron lasers (FELs) are the unique sources of intense and tunable radiation in far-IR (THz) and submillimeter range and are often used for EPR investigation of paramagnetic species at extremely high frequencies and magnetic fields.[36−38] The experiment proposed by us here, however, makes use of THz light not for the excitation of EPR transitions but for inducing vibrational transitions with simultaneous control of spin states by EPR. We report the study of the influence of high-power THz radiation on the relaxation processes in switchable molecular magnet Cu-(hfac)$_2$L^{Pr}. Far-IR spectra of this compound have intense absorption lines different for ground (**G**) and metastable (**M**) geometries; therefore, these lines can be examined by THz radiation generated by high-power FEL. In the following sections, we describe the assembled experimental setup and choice of THz frequencies for sample irradiation on the basis of its far-IR spectra, investigate the influence of intense THz pulses on the spin state of studied molecular magnet at different THz frequencies, and discuss the obtained results.

EXPERIMENTAL SECTION

Free Electron Laser. The Novosibirsk free electron laser (NovoFEL) is one of the most intense radiation sources in the THz spectral range.[39] It generates continuous train 100 ps pulses with a repetition rate of up to 22.4 MHz (5.6 MHz in routine mode) and an average THz power of up to 500 W (up to 0.6 MW peak power). The radiation wavelength can be precisely tuned from 110 to 235 μm (~90–40 cm^{-1}, first stage) and from 35 to 80 μm (~280–120 cm^{-1}, second stage), whereas the relative line width of radiation is ~0.2 to 1%. The smaller value of the line width corresponds to the Fourier transform limit for experimentally measured THz micropulses of 100 ps fwhm duration (Figure 4a). The laser radiation is

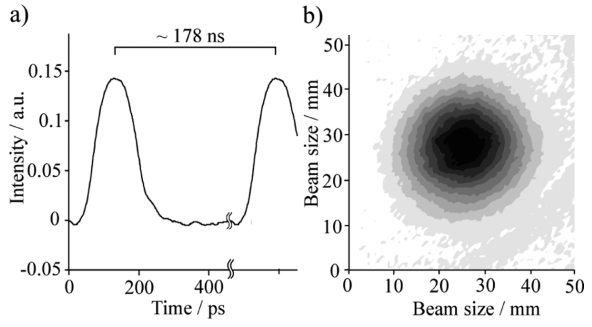

Figure 4. (a) Shape and repetition rate of the THz pulses in routine mode. Duration of the pulse is ~100 ps. (b) Laser beam intensity profile at $1/\lambda \approx 200$ cm^{-1}.

linearly polarized and completely spatially coherent. The laser beam intensity profile has a Gaussian shape. For the second stage used in this work, the beam intensity profile is shown in the Figure 4b.

THz radiation is transmitted to the user stations through the beamline filled with dry air–nitrogen mixture. It is necessary for diminishing of the radiation absorption by the water vapor.

dx.doi.org/10.1021/jp311404t | J. Phys. Chem. A 2013, 117, 1483–1491

EPR Spectrometer. To perform the EPR detection, an experimental station based on the CW electron paramagnetic resonance spectrometer operating at ∼9 GHz (X-band) has been assembled by the THz beamline of the NovoFEL. Spectrometer consists of the following parts. Permalloy-based low-resistance (3 Ohm) electromagnet has an interpolar distance of 56 mm and is able to produce the magnetic field of up to 0.8 T. To produce and control the magnetic field, the Lambda GEN60−25 power supply and LakeShore 455 gaussmeter equipped with a Hall-probe HMNT-4E04-VF were used. The microwave bridge was a part of commercially available on-table EPR spectrometer (EPR-10 mini, Russia), whereas the Bruker ER 4118X-MD5 resonator was used as a probe. Microwave frequency was controlled by the Agilent 53131A-124 frequency counter. The output mw power of the bridge was calibrated using HP 463A power meter and lied in the range of 10−15 mW for all experiments. The detection of the EPR signal was done using SR830 lock-in amplifier. The G3-112/1 amplifier was used to amplify a modulation sine wave of the SR830 and allowed us to achieve the modulation amplitude of up to 4 Gs; however, the modulation amplitude of 2 Gs was sufficient and was used in all experiments. For control of EPR spectrometer the fsc2 program was used (web page: www.fsc2.org). fsc2 reads out the EPR signal from the SR830 lock-in amplifier and controls magnetic field through the input/output ports of the SR830, which are connected to the field controller and magnet power supply. EPR spectrometer was equipped with the Oxford Instruments temperature control system based on an ER-4118CF cryostat and an ITC503 temperature controller which allowed us to perform EPR experiments in the temperature range of 4−300 K.

Irradiation of the Sample in the Resonator of EPR Spectrometer with near-IR Light and THz Radiation. During the EPR experiments, two different types of laser radiation can be used to irradiate the sample: Nd:YaG laser at 1064 nm and FEL operating in the range of 35−80 μm. To irradiate the sample with near-IR light (1064 nm), a standard pathway for the light through the quartz windows of the cryostat was used. Nd:YaG laser operates in a free run mode when a Q-switch is permanently open and the laser pulse has duration of ∼100 μs. This operation mode was used to prevent local overheating of the sample during the laser pulse. The repetition rate of the laser pulses was 10 Hz for all experiments performed with the beam power of 45 mJ per pulse on the output of the laser. Optical elements used in cryostat (quartz windows) and EPR resonator (sapphire ring) are not transparent for THz wavelengths used in experiments ($\lambda \sim 50$ μm). Thus, the only way to irradiate the sample directly into the EPR resonator was to use a sample holder, which also played a role of waveguide for THz radiation. Instead of standard sample holder (a rod of ∼60 cm length and 8 mm in diameter), a glass tube of the same outer diameter and similar length was used. The inner diameter of the tube was 6 mm. The sample size was limited to 5 mm maximum in diameter for the EPR resonator used; therefore, the glass tube had a narrowing to 4 mm (outer diameter) at one of the ends to fit the sample into the resonator. Tollens' reagent was used to apply a silver mirror to the inner surface of the tube, making it reflective for the THz radiation. The only part of the inner surface of the tube that was free of the silver mirror was the narrowed end of the tube positioned in the EPR resonator (Figure 5a). When the sample holder tube was aligned with the THz beam, the ratio between outcoming and incoming THz power in the tube was equal to ∼0.2. This value was roughly 1.5 times higher than the ratio of output to input hole areas, indicating reasonable waveguide efficiency. The THz power was measured by a Gentec-EO UP19K-15S-VR detector preliminary calibrated for THz frequencies used in experiments. THz power indicated below corresponds to the power measured at the entrance of the sample holder.

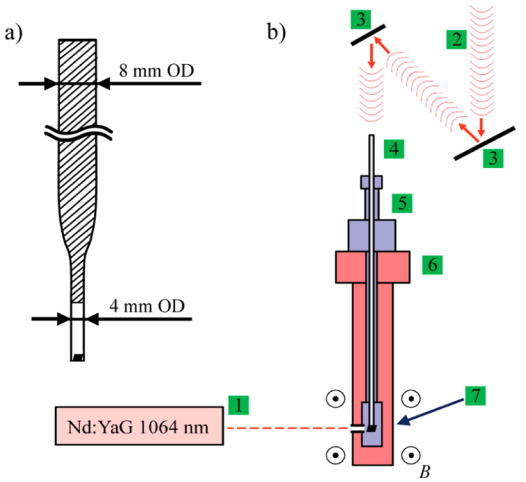

Figure 5. (a) Sketch of the sample holder used for THz irradiation. Grid lines show silver mirror coating. (b) Irradiation scheme of the experiment. All parts of the EPR spectrometer except cryostat and resonator are omitted. (1) Nd:YaG laser, (2) THz beam, (3) flat copper mirrors, (4) sample holder, (5) probehead of the EPR resonator, (6) EPR cryostat, and (7) sample inside the EPR resonator.

The studied compound was placed on the bottom of the sample tube, which was covered with polyethylene film cap transparent for both THz and near-IR radiation. As a result, during the EPR experiment, any of two radiation sources could be used to irradiate the sample. The quasi-optical system based on two flat copper mirrors was attached to the THz beamline to align the THz beam with the sample holder waveguide (Figure 5b). A metal shutter (not shown in Figure 5b) was used to control the THz irradiation of the sample.

Measurements of the Far-IR Spectra of Studied Compound. As was previously mentioned, polymer−chain complex $Cu(hfac)_2L^{Pr}$ studied in this work undergoes temperature-induced structural rearrangements accompanied by magnetic moment changes. To obtain its far-IR spectra, a Bruker IFS 125 HR FT-IR spectrometer equipped with helium cryostat was used. The spectra were measured at temperatures 250 and 4 K and correspond to high- and low-temperature structure of $Cu(hfac)_2L^{Pr}$, respectively. To prepare the sample for far-IR measurements, a mixture of 50 mg of high-density polyethylene (HDPE) powder with a 5 mg of $Cu(hfac)_2L^{Pr}$ powder was compressed into a pellet at pressure of 5 tons. Far-IR spectra were measured in the range of 100−400 cm^{-1} with a spectral resolution of 1 cm^{-1}.

RESULTS AND DISCUSSION

Characteristic Absorption Lines of the $Cu(hfac)_2L^{Pr}$ Compound in the THz Frequency Range. Far-IR spectra of the $Cu(hfac)_2L^{Pr}$ measured in the frequency range of 100−400 cm^{-1} at T = 250 and 4 K are shown in Figure 6a.

As the temperature decreases, the absorption lines narrow and most of them retain their positions in the spectra. Nevertheless, the relative intensity of some of them becomes

dx.doi.org/10.1021/jp311404t | J. Phys. Chem. A 2013, 117, 1483−1491

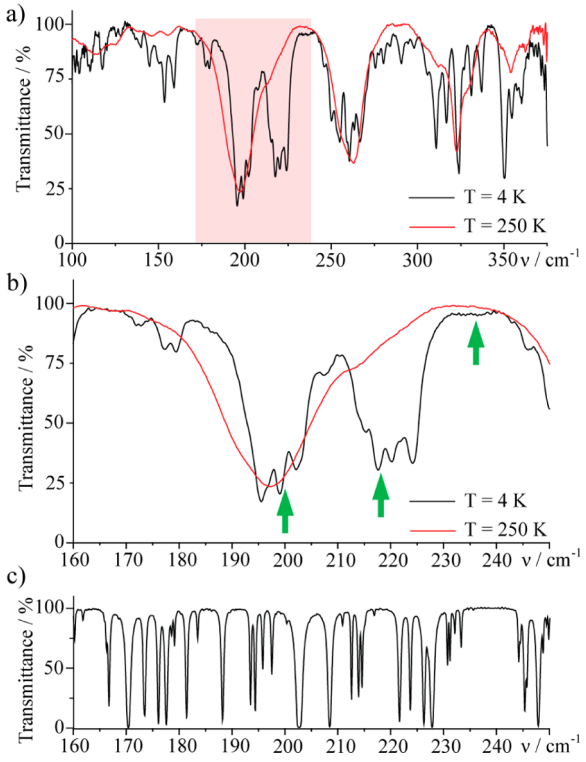

Figure 6. (a) Far-IR spectra of $Cu(hfac)_2L^{Pr}$ compound at temperatures 250 and 4 K. (b) Magnified spectral region where the new intense absorption line appears below phase transition. Arrows show the frequencies at which the sample was irradiated by THz power in the following experiments. (c) Far-IR spectra of atmosphere under ambient conditions. Water vapor absorption lines are recorded.

smaller and rise of new intense lines is observed. The part of the far-IR spectra where new lines appeared is shown in Figure 6b. At high temperature (250 K), only one intense line centered at ∼200 cm^{-1} is present in the range of 160−240 cm^{-1}, whereas at low temperature (4 K) there are two lines (∼200 and ∼220 cm^{-1}) with quite similar intensity. The assignment of the above-mentioned absorption lines to certain vibration modes that can be done for simple molecules such as Cu−C−O,[40] is hardly possible for the studied complex due to its complicated structure. Nevertheless, on the basis of X-ray data one assumes that at high temperature the intense line at ∼200 cm^{-1} is due to absorption by both coordination units CuO_4N_2 and CuO_6. Below phase transition the CuO_4N_2 unit retains the same geometry, whereas CuO_6 undergoes significant structural rearrangements. In agreement with X-ray data, at low temperature the absorption line at ∼200 cm^{-1} is still found at the same position (corresponds to CuO_4N_2 units), and the new line of comparable intensity appears due to the structural rearrangements (corresponds to CuO_6 units). Thus, the spin triad at HT geometry (T = 250 K) has the absorption line at ∼200 cm^{-1}, whereas the same triad at LT geometry (T = 4 K) intensively absorbs at ∼220 cm^{-1}. As was mentioned in the Introduction, the light-induced switching of the spin triad converts it from LT to HT geometry (**G**→**M** state conversion), which should lead to the transfer of the absorption intensity from 220 to 200 cm^{-1}. Thereby there are three important frequencies marked by arrows in Figure 6b, which should be probed by THz irradiation: two of them correspond to the characteristic absorption lines of spin triad at ∼200 and ∼220 cm^{-1}, and the third one at ∼235 cm^{-1} corresponds to the case where studied compound is almost transparent (no absorption is detected). When selecting the THz frequencies for experiments, the transparency of the atmosphere was taken into account to avoid unwanted absorption of the radiation by water vapor (Figure 6c).

Below, we present two different types of experiments. The first one is focused on the study of the quality of THz radiation waveguide and on THz absorption selectivity depending on radiation frequency. The second one investigates the influence of THz radiation on the spin state of spin triad in stable (**G**) and photoinduced metastable (**M**) states. In both cases, a single crystal of $Cu(hfac)_2L^{Pr}$ compound was used aiming to simplify interpretation of the EPR spectra compared with powder sample, but the size of the crystals in these experiments was different. For the first type a single crystal of typical size ∼1 × 1 × 2 mm was used, whereas for the second type a thin plate with a thickness of ∼100−200 μm and ∼1 mm^2 square was selected. Crystal of such thickness was transparent enough for the 1064 nm light and allowed us to perform photoswitching in the whole crystal volume. It should be mentioned that thin plate used in experiments is also quite transparent for THz radiation because it is approximately two times thinner than effective thickness of sample in pellet prepared for far-IR measurements (Figure 6a); therefore, at energies of ∼200 and 220 cm^{-1} it absorbs approximately 20−40% of incident THz irradiation. At the same time, single crystal for the first type of experiments is ∼10 times thicker and absorbs most of the incident THz radiation at the same energies.

Absorption Selectivity of $Cu(hfac)_2L^{Pr}$ Depending on Frequency in the THz Range. Figure 7 shows EPR spectra of

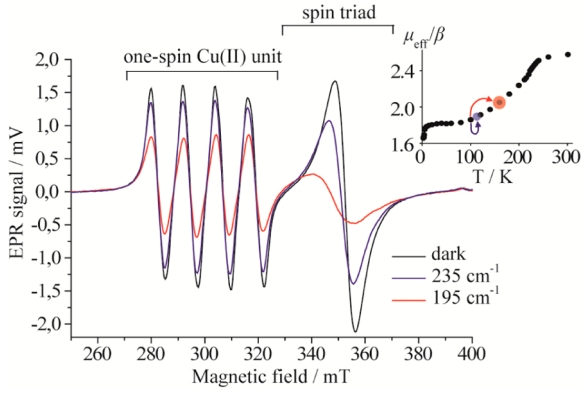

Figure 7. EPR spectra of single crystal of $Cu(hfac)_2L^{Pr}$ (arbitrary orientation) measured in X-band (ν_{mw} ≈ 9.73 GHz) at temperature T = 100 K: without THz irradiation (black line), 55 mW irradiation at 195 cm^{-1} (red line), and 55 mW irradiation at 235 cm^{-1} (blue line). Inset shows μ_{eff} changes of the sample corresponding to the temperature changes at 195 cm^{-1} irradiation (red line) and 235 cm^{-1} irradiation (blue line).

$Cu(hfac)_2L^{Pr}$ (single crystal) measured at T = 100 K. EPR spectra consist of two signals corresponding to two types of paramagnetic centers: one-spin copper(II) ions (in coordination units CuO_4N_2) and spin triads nitroxide-copper(II)-nitroxide (in coordination units CuO_6). Position and shape of the former signal does not depend on temperature (except for relaxation broadening/narrowing), whereas for the latter one the dependence is crucial due to reversible structural rearrangements taking place in spin triads during phase transition.[27,28]

dx.doi.org/10.1021/jp311404t | J. Phys. Chem. A 2013, 117, 1483−1491

Incident THz irradiation leads to the heating of the sample, and the resulting sample temperature depends on the power of radiation and sample absorption efficiency. To investigate selectivity of THz absorption by a sample, according to its far-IR spectra, the sample was irradiated at 195 and 235 cm^{-1} with the incident power of 55 mW (at the entrance to waveguide tube). The temperature of the EPR resonator does not change during experiments. The sample temperature, however, may change due to the THz power being absorbed. In this case, EPR signal intensity during THz irradiation is described by Boltzmann population in the spin system, depending on temperature. The intensity of the EPR signal of one-spin copper(II) unit can be used to monitor the sample temperature changes by means of eq 1:

$$\frac{I_{T_1}}{I_{T_2}} = \frac{(1 - \exp^{-g\beta B/kT_1})}{(1 - \exp^{-g\beta B/kT_2})} \approx \frac{T_2}{T_1} \quad (1)$$

where I_T is an integral intensity of the EPR signal at certain temperature, T is a temperature of the sample, g is a g-factor, B is magnetic field, and k is Boltzmann constant. Simulations of experimental spectra (see the Supporting Information for details) allowed us to obtain integral intensities of signals corresponding to the one-spin Cu(II) unit; then, using eq 1 we could estimate that the sample temperature increases from 100 to 113 ± 2 K during irradiation at 235 cm^{-1} and from 100 to 159 ± 10 K during irradiation at 195 cm^{-1}. Therefore, the sample absorbs much more THz radiation when its frequency corresponds to far-IR absorption band of the studied compound. Nevertheless, in the case of 235 cm^{-1}, where the sample has no intense absorption lines, its temperature still increases during radiation. One of the possible explanations is a heating of the glass wall of the sample holder by incident THz radiation. Indeed, the end of the sample holder tube is free of silver mirror to be transparent for the mw radiation in EPR resonator, and this part of the tube can absorb THz radiation quite effectively because the glass is not transparent in the far-IR region. Nevertheless, it is evident that the heating of the sample is much more pronounced when the radiation frequency corresponds to far-IR absorption bands.

Influence of THz Radiation on Three-Spin Cluster in Ground and Metastable State. Thin plate single crystal of $Cu(hfac)_2L^{Pr}$ was used in the experiments described below to afford efficient photoswitching in the whole sample volume by 1064 nm light. First, possible influence of THz radiation on the ground state **G** (before photoswitching) of the sample was studied at low temperature (5 K). Figure 8 shows EPR spectra of the studied compound with THz radiation on/off for radiation frequencies corresponding to intense absorption lines (~200 and ~218 cm^{-1}) and THz transparent region (~236 cm^{-1}).

In all three cases, EPR spectra retain the same shape but have slightly smaller intensity compared with the dark spectrum (THz off). Thus, no effect of THz radiation was detected except for moderate heating of the sample; in all three cases, the temperature of the sample did not exceed 8 K ($\Delta T_{max} \approx 2.5$ K at 218 cm^{-1}). The heating effect was smallest during ~236 cm^{-1} irradiation ($\Delta T \approx 0.7$ K) because the $Cu(hfac)_2L^{Pr}$ complex has no intense absorption lines (even though the THz power at ~236 cm^{-1} was significantly higher than that at ~200 and ~218 cm^{-1}). Therefore, in the case of the thin plate sample we also conclude that the direct absorption of THz radiation dominates over the indirect heating of the sample by its environment.

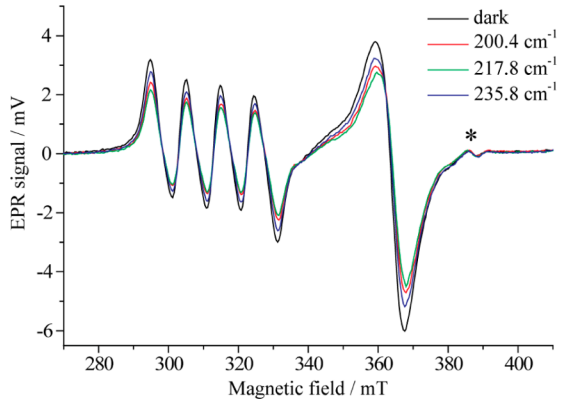

Figure 8. EPR spectra of thin plate single crystal of $Cu(hfac)_2L^{Pr}$ (arbitrary orientation) measured in X-band ($\nu_{mw} \approx$ 9.74 GHz) at temperature T = 5 K: without THz irradiation (black line), 30 mW irradiation at 200.4 cm^{-1} (red line), 40 mW irradiation at 217.8 cm^{-1} (green line), and 55 mW irradiation at 235.8 cm^{-1} (blue line). Asterisk marks background signal of EPR resonator.

As has been previously shown,[34] the heating of photoswitched sample leads to immediate decrease in the fraction of **M** states and acceleration of the relaxation to the ground **G** state. Therefore, in principle, a simple heating by THz power can also accelerate **M**→**G** conversion without proceeding via the mechanism shown in Figure 3a (red arrow). However, the heating induced by THz absorption in our experimental conditions (Figure 8) is very moderate; therefore, most of the clusters in the **M** state are expected to remain in their metastable geometry. Thus, once a significant acceleration of **M**→**G** conversion induced by THz radiation is observed, it could definitely be attributed to relaxation processes via selective excitation of characteristic vibrational levels of the system (mechanism shown in Figure 3a).

To investigate this possibility experimentally, we used the following sequence of experiments (Figure 3b). (I) First, the single crystal of the $Cu(hfac)_2L^{Pr}$ compound has been cooled to 5 K in the EPR resonator in the dark and its EPR spectrum has been recorded. (II) Then, the sample has been irradiated with 1064 nm light to induce conversion to the metastable **M** state. (III) After switching the 1064 nm light off, the EPR spectrum of **M** state has been recorded to confirm the photoswitching. (IV) Then, the sample has been irradiated with THz light with the EPR detection during radiation. (V) After switching the THz radiation off, the EPR spectrum has been recorded again. (VI) (not shown in Figure 3b). The temperature of the cryostat has been increased to 25 K to convert all of the spin triads to the ground **G** state and then lowered back to 5 K. Finally, the EPR spectrum has been recorded again at 5 K for comparison with that measured before the experimental cycle.

Excitation of $Cu(hfac)_2L^{Pr}$ at 5 K using 1064 nm light changes EPR spectrum significantly. Figure 9 compares dark spectrum (a) and spectrum after 1 min of irradiation with 1064 nm light (b). EPR signal of isolated copper(II) ion has no observable changes except for the region overlapped with the signal of spin triad. Contrary to that, the signal of spin triad changes its intensity and position in the spectrum significantly and resembles HT EPR spectrum (Figure 7, red).[33] After the 1064 nm light is off, the EPR spectrum slowly relaxes toward its initial low-temperature shape.[34] As was mentioned in the

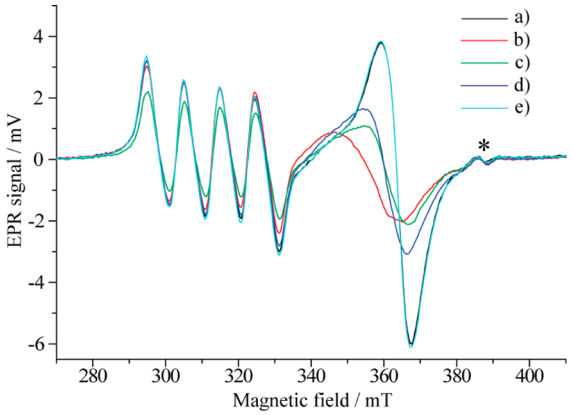

Figure 9. EPR spectra of thin plate single crystal of $Cu(hfac)_2L^{Pr}$ (arbitrary orientation) at temperature 5 K measured in X-band ($\nu_{mw} \approx$ 9.74 GHz): (a) initial spectrum, (b) immediately after 1 min of 1064 nm laser excitation, (c) during irradiation by 40 mW THz power at 200.4 cm^{-1}, (d) after THz radiation is switched off, and (e) after warming the irradiated sample up to 25 K and then cooling back to 5 K. Asterisk marks signal from EPR resonator.

Introduction, this relaxation process is strongly temperature-dependent and at 5 K takes a few hours; therefore, we can safely neglect it as a full experimental cycle (steps I–VI in Figure 3b) takes less than 10 min. After photoswitching at 1064 nm and recording the EPR spectrum, the sample has been exposed to THz radiation at 200.4 cm^{-1}, which was expected to be absorbed by both photoswitched spin triads and isolated copper(II) ions. Simultaneously, EPR spectrum of the sample has been recorded (Figure 9c). The decrease in the signal of isolated copper(II) ion allows us to estimate the heating of the sample by THz power to $T \approx 7.5$ K. As was previously mentioned, this heating leads to a slight decrease in steady-state ratio between **G** and **M** states (**M** fraction decreases with an increase in T);[34] therefore, the EPR signal of the three-spin clusters moves toward its LT position corresponding to **G** state. However, THz radiation does not induce complete or significant relaxation of the photoswitched spin triads from **M** to **G** state. When THz irradiation is switched off, the temperature of the sample returns to 5 K and EPR signal intensity increases, whereas its position and shape remain the same (Figure 9d). To restore the EPR spectrum completely, the temperature of the sample should have been increased to 25 K by means of cryostat heater and then lowered back to 5 K. The EPR spectrum recorded after this completely coincides with the initial one (Figure 9, e).

Similar photoswitching experiments performed with the THz irradiation at 235.8 and 217.8 cm^{-1} have shown the same tendency: the absence of complete relaxation of the photoswitched spin triads to the ground **G** state and the acceleration of relaxation corresponding to the temperature increase.

Summarizing the results of the experiments performed, one concludes that (i) the investigated compound $Cu(hfac)_2L^{Pr}$ absorbs THz radiation, in agreement with its far-IR spectra and can be significantly warmed up into the EPR resonator by THz pulses, and (ii) the excitation of the selected vibrational levels of the spin triads in metastable geometry does not lead to reverse **M***→**G** relaxation, and the main effect of THz irradiation is the heating of the sample due to vibrational relaxation. There are two possible explanations for the second observation. Either the vibrations excited by THz radiation are not associated with reaction coordinate of the **M***→**G** conversion or the intermodal vibrational relaxation **M***→**M** is too fast in comparison with **M***→**G** conversion ($k_1 \gg k_2$). Indeed, only a few of many characteristic absorption lines in the far-IR region have been probed by the THz laser because it is almost impossible to check every line using FEL-based THz source. (The high-power broadband synchrotron radiation tuned to far-IR region, probably, is more suitable in this respect.) Vibrational relaxation processes have been actively studied during the last decades using femtosecond spectroscopy.[41] In particular, it has been found that vibrational relaxation times strongly depend on compound and its state (solid or liquid) but in most cases are found in the range of ~100 fs to ~1 ps.[42−45] We should stress that the above-mentioned relaxation times were measured for compounds of significantly different structure compared with polymer-chain complex $Cu(hfac)_2L^{Pr}$; the vibrational relaxation times in the latter have not yet been studied but are not expected to exceed 1 ps ($k_1 \approx 10^{12}$ s^{-1}). At the same time, the effective rate constant k_2 for thermally populated vibrational states at room temperature ($kT \approx 200$ cm^{-1}) is expected to be on the order of 10^9 s^{-1} for iron(II) spin-crossover complexes.[46] The k_2 value has not been known for studied compound $Cu(hfac)_2L^{Pr}$ in advance, but the experiments performed here allow us to conclude that $k_2 \ll k_1$. Supposedly, this is the main reason why the **M***→**M** relaxation dominates over the **M***→**G** processes in our experiments.

CONCLUSIONS AND OUTLOOK

To investigate the influence of intense THz radiation on spin state and geometry of the photoswitchable $Cu(hfac)_2L^{Pr}$ compound, the X-band EPR spectrometer has been assembled by the THz beamline of the free electron laser NovoFEL. The use of specially designed sample holder allowed us to irradiate the studied compound using the Nd:YaG (1064 nm) and THz (500−100 cm^{-1}) laser radiation directly in the EPR resonator. Far-IR spectra measured for the $Cu(hfac)_2L^{Pr}$ compound at high (250 K) and low (4 K) temperatures show characteristic absorption lines corresponding to the high- and low-temperature geometries and having frequencies in the THz range accessible by NovoFEL. The efficiency of direct absorption of the THz energy by the studied compound inside the EPR resonator has been confirmed: the temperature of the sample increases significantly when the THz frequency fits to the absorption line of the sample. Photoswitching of the spin triads of $Cu(hfac)_2L^{Pr}$ at 5 K by the 1064 nm light and subsequent irradiation of the sample by THz frequency did not reveal selective influence of THz radiation on the conversion from metastable to stable states. Supposedly, this occurs due to the fast vibrational relaxation processes taking less than a few picoseconds, which are much faster than the conversion of the vibrational excited metastable state to the ground state.

Although the selective influence of THz radiation on spin states of molecular magnets $Cu(hfac)_2L^{Pr}$ has not been found in this work, the observed heating phenomena are quite interesting and promising for future developments. The ability of high-power THz pulses for fast and significant increase in the sample temperature without its destruction and interference with quantum effects can be used in number of experiments. For instance, the fast switching of spin states in spin crossover compounds near the transition temperature (or within the hysteresis loop) can be studied. Another point is that after switching the THz radiation off, the sample positioned inside the helium-cooled cryostat should experience extremely fast cooling, which is advantageous for studying temperature-

dx.doi.org/10.1021/jp311404t | J. Phys. Chem. A 2013, 117, 1483−1491

induced excited spin state trapping (TIESST)[47,48] and similar phenomena. In terms of EPR technology, one may also think of new temperature-induced EPR experiments. These and other approaches based on pulse selective THz power heating and EPR detection will be elaborated in our future research.

■ ASSOCIATED CONTENT

Supporting Information

Simulation details of the experimental spectra shown in Figure 7. This material is available free of charge via the Internet at http://pubs.acs.org.

■ AUTHOR INFORMATION

Corresponding Author

*E-mail: sergey.veber@tomo.nsc.ru.

Notes

The authors declare no competing financial interest.

■ ACKNOWLEDGMENTS

This work was supported by the Russian Foundation for Basic Research (nos. 11-03-00158, 12-03-33010, and 12-03-31396), the RF President's Grant (MK-1662.2012.3, MK-1165.2012.3), the Grant for the Leading Scientific Schools (NSh-2429.2012.3), and the Ministry of education and science of Russian Federation (projects 8436 and 8456). We are very thankful to Dr. Jens T. Torring (FU, Berlin) for the fsc2 program used to control the EPR spectrometer. This work was carried out with the involvement of equipment belonging to the shared research center "SSTRC" and supported by the Ministry of education and science of the Russian Federation.

■ REFERENCES

(1) Kahn, O. *Molecular Magnetism*; VCH: New York, 1993.
(2) *Molecular Magnetism: From Molecular Assemblies to the Devices*; NATO ASI Series, E: Applied Sciences; Coronado, E.; Delhaés, P., Gatteschi, D., Miller, J. S., Eds.; Kluwer Academic Publisher: Dordrecht, The Netherlands, 1996; Vol. *321*.
(3) *Spin Crossover in Transition Metal Compounds*; Gütlich, P., Goodwin, H. A., Eds.; Topics in Current Chemistry; Springer-Verlag: New York, 2004; Vols. *I–III*, pp 233–235.
(4) Decurtins, S.; Gutlich, P.; Kohler, C. P.; Spiering, H.; Hauser, A. *Chem. Phys. Lett.* **1984**, *105*, 1–4.
(5) Gutlich, P.; Hauser, A.; Spiering, H. *Angew. Chem., Int. Ed. Engl.* **1994**, *33*, 2024–2054.
(6) Sato, O. *Acc. Chem. Res.* **2003**, *36*, 692–700.
(7) Bousseksou, A.; Molnar, G.; Salmon, L.; Nicolazzi, W. *Chem. Soc. Rev.* **2011**, *40*, 3313–3335.
(8) Dei, A.; Gatteschi, D. *Angew. Chem., Int. Ed.* **2011**, *50*, 11852–11858.
(9) Sato, O.; Tao, J.; Zhang, Y.-Z. *Angew. Chem.* **2007**, *119*, 2200–2236; *Angew. Chem., Int. Ed.* **2007**, *46*, 2152–2187.
(10) Sessoli, R. *Nat. Chem.* **2010**, *2*, 346–347.
(11) Benelli, C.; Gatteschi, D. *Chem. Rev.* **2002**, *102*, 2369–2387.
(12) Luneau, D.; Rey, P. *Coord. Chem. Rev.* **2005**, *249*, 2591–2611.
(13) Musin, R. N.; Schastnev, P. V.; Malinovskaya, S. A. *Inorg. Chem.* **1992**, *31*, 4118–4121.
(14) Caneschi, A.; Gatteschi, D.; Rey, P. *Prog. Inorg. Chem.* **1991**, *39*, 331.
(15) Caneschi, A.; Gatteschi, D.; Laugier, J.; Rey, P. *J. Am. Chem. Soc.* **1987**, *109*, 2191.
(16) Laugier, J.; Rey, P.; Benelli, C.; Gatteschi, D.; Zanchini, C. *J. Am. Chem. Soc.* **1986**, *108*, 6931.
(17) Gatteschi, D.; Laugier, J.; Rey, P.; Zanchini, C. *Inorg. Chem.* **1987**, *26*, 938.
(18) dePanthou, F. L.; Belorizky, E.; Calemczuk, R.; Luneau, D.; Marcenat, C.; Ressouche, E.; Turek, P.; Rey, P. *J. Am. Chem. Soc.* **1995**, *117*, 11247–11253.
(19) Caneschi, A.; Chiesi, P.; David, L.; Ferraro, F.; Gatteschi, D.; Sessoli, R. *Inorg. Chem.* **1993**, *32*, 1445–1453.
(20) Ovcharenko, V. I.; Fokin, S. V.; Romanenko, G. V.; Shvedenkov, Yu. G.; Ikorskii, V. N.; Tretyakov, E. V.; Vasilevskii, S. F. *J. Struct. Chem.* **2002**, *43*, 153–167.
(21) Ovcharenko, V. I.; Maryunina, K. Yu.; Fokin, S. V.; Tretyakov, E. V.; Romanenko, G. V.; Ikorskii, V. N. *Russ. Chem. Bull., Int. Ed.* **2004**, *53*, 2406–2427.
(22) Ovcharenko, V. I.; Romanenko, G. V.; Maryunina, K. Yu.; Bogomyakov, A. S.; Gorelik, E. V. *Inorg. Chem.* **2008**, *47*, 9537–9552.
(23) Romanenko, G. V.; Maryunina, K. Yu.; Bogomyakov, A. S.; Sagdeev, R. Z.; Ovcharenko, V. I. *Inorg. Chem.* **2011**, *50*, 6597–6609.
(24) Fedin, M. V.; Veber, S. L.; Maryunina, K. Yu.; Romanenko, G. V.; Suturina, E. A.; Gritsan, N. P.; Sagdeev, R. Z.; Ovcharenko, V. I.; Bagryanskaya, E. G. *J. Am. Chem. Soc.* **2010**, *132*, 13886–13891.
(25) Fedin, M.; Veber, S.; Gromov, I.; Ovcharenko, V.; Sagdeev, R.; Schweiger, A.; Bagryanskaya, E. *J. Phys. Chem. A* **2006**, *110*, 2315–2317.
(26) Fedin, M.; Veber, S.; Gromov, I.; Ovcharenko, V.; Sagdeev, R.; Bagryanskaya, E. *J. Phys. Chem. A* **2007**, *111*, 4449–4455.
(27) Fedin, M.; Veber, S.; Gromov, I.; Maryunina, K.; Fokin, S.; Romanenko, G.; Sagdeev, R.; Ovcharenko, V.; Bagryanskaya, E. *Inorg. Chem.* **2007**, *46*, 11405–11415.
(28) Veber, S. L.; Fedin, M. V.; Potapov, A. I.; Maryunina, K. Yu.; Romanenko, G. V.; Sagdeev, R. Z.; Ovcharenko, V. I.; Goldfarb, D.; Bagryanskaya, E. G. *J. Am. Chem. Soc.* **2008**, *130*, 2444–2445.
(29) Veber, S. L.; Fedin, M. V.; Maryunina, K. Yu.; Romanenko, G. V.; Sagdeev, R. Z.; Bagryanskaya, E. G.; Ovcharenko, V. I. *Inorg. Chim. Acta* **2008**, *361*, 4148–4152.
(30) Fedin, M. V.; Veber, S. L.; Romanenko, G. V.; Ovcharenko, V. I.; Sagdeev, R. Z.; Klihm, G.; Reijerse, E.; Lubitz, W.; Bagryanskaya, E. G. *Phys. Chem. Chem. Phys.* **2009**, *11*, 6654–6663.
(31) Fedin, M. V.; Veber, S. L.; Sagdeev, R. Z.; Ovcharenko, V. I.; Bagryanskaya, E. G. *Russ. Chem. Bull., Int. Ed.* **2010**, *59*, 1065–1079.
(32) Veber, S. L.; Fedin, M. V.; Maryunina, K. Yu.; Potapov, A.; Goldfarb, D.; Reijerse, E.; Lubitz, W.; Sagdeev, R. Z.; Ovcharenko, V. I.; Bagryanskaya, E. G. *Inorg. Chem.* **2011**, *50*, 10204–10212.
(33) Fedin, M.; Ovcharenko, V.; Sagdeev, R.; Reijerse, E.; Lubitz, W.; Bagryanskaya, E. *Angew. Chem., Int. Ed.* **2008**, *47*, 6897–6899; *Angew. Chem.* **2008**, *120*, 7003–7005.
(34) Fedin, M. V.; Maryunina, K. Y.; Sagdeev, R. Z.; Ovcharenko, V. I.; Bagryanskaya, E. G. *Inorg. Chem.* **2012**, *51*, 709–717.
(35) Fedin, M. V.; Bagryanskaya, E. G.; Matsuoka, H.; Yamauchi, S.; Veber, S. L.; Maryunina, K. Y.; Tretyakov, E. V.; Ovcharenko, V. I.; Sagdeev, R. Z. *J. Am. Chem. Soc.* **2012**, *134*, 16319–16326.
(36) Zvyagin, S. A.; Ozerov, M.; Cizmar, E.; Kamenskyi, D.; Zherlitsyn, S.; Herrmannsdorfer, T.; Wosnitza, J.; Wuensch, R.; Seidel, W. *Rev. Sci. Instrum.* **2009**, *80*, 073102.
(37) Takahashi, S.; Allen, D. G.; Seifter, J.; Ramian, G.; Sherwin, M. S.; Brunel, L. C.; van Tol, J. *Infrared Phys. Technol.* **2008**, *51*, 426–428.
(38) Schnegg, A.; Behrends, J.; Lips, K.; Bittl, R.; Holldack, K. *Phys. Chem. Chem. Phys.* **2009**, *11*, 6820–6825.
(39) Gavrilov, N. G.; Knyazev, B. A.; Kolobanov, E. I.; Kotenkov, V. V.; Kubarev, V. V.; Kulipanov, G. N.; Matveenko, A. N.; Medvedev, L. E.; Miginsky, S. V.; Mironenko, L. A.; et al. *Nucl. Instrum. Methods Phys. Res., Sect. A* **2007**, *575*, 54–57.
(40) Tremblay, B.; Manceron, L. *Chem. Phys.* **1999**, *242*, 235–240.
(41) Zewail, A. H. *J. Phys. Chem. A* **2000**, *104*, 5660–5694.
(42) Rhinehart, J. M.; Challa, J. R.; McCamant, D. W. *J. Phys. Chem. B* **2012**, *116*, 10522–10534.
(43) Preston, T. J.; Dutta, M.; Esselman, B. J.; Kalume, A.; George, L.; McMahon, R. J.; Reid, S. A.; Crim, F. F. *J. Chem. Phys.* **2011**, 135.
(44) Jarota, A.; Tondusson, M.; Galle, G.; Freysz, E.; Abramczyk, H. *J. Phys. Chem. A* **2012**, *116*, 4000–4009.
(45) van der Veen, R. M.; Cannizzo, A.; van Mourik, F.; Vlcek, A.; Chergui, M. *J. Am. Chem. Soc.* **2011**, *133*, 305–315.

(46) Hauser, A. *Spin Crossover in Transition Metal Compounds II*; Gütlich, P., Goodwin, H. A., Eds.; Topics in Current Chemistry; Springer: London, 2004; Vol. *234*, pp 155−198.
(47) Avendano, C.; Hilfiger, M. G.; Prosvirin, A.; Sanders, C.; Stepien, D.; Dunbar, K. R. *J. Am. Chem. Soc.* **2010**, *132*, 13123−13125.
(48) Craig, G. A.; Costa, J. S.; Roubeau, O.; Teat, S. J.; Aromi, G. *Chem.—Eur. J.* **2011**, *17*, 3120−3127.